JCI insight

Role of adenylyl cyclase 6 in the development of lithium-induced nephrogenic diabetes insipidus

Søren Brandt Poulsen, … , Timo Rieg, Robert A. Fenton

JCI Insight. 2017;2(7):e91042. https://doi.org/10.1172/jci.insight.91042.

Research Article Cell biology

Psychiatric patients treated with lithium (Li^+) may develop nephrogenic diabetes insipidus (NDI). Although the etiology of Li^+-induced NDI (Li-NDI) is poorly understood, it occurs partially due to reduced aquaporin-2 (AQP2) expression in the kidney collecting ducts. A mechanism postulated for this is that Li^+ inhibits adenylyl cyclase (AC) activity, leading to decreased cAMP, reduced AQP2 abundance, and less membrane targeting. We hypothesized that Li-NDI would not develop in mice lacking AC6. Whole-body AC6 knockout ($AC6^{-/-}$) mice and potentially novel connecting tubule/principal cell–specific AC6 knockout ($AC6^{loxloxCre}$) mice had approximately 50% lower urine osmolality and doubled water intake under baseline conditions compared with controls. Dietary Li^+ administration increased water intake and reduced urine osmolality in control, $AC6^{-/-}$, and $AC6^{loxloxCre}$ mice. Consistent with $AC6^{-/-}$ mice, medullary AQP2 and pS256-AQP2 abundances were lower in $AC6^{loxloxCre}$ mice compared with controls under standard conditions, and levels were further reduced after Li^+ administration. $AC6^{loxloxCre}$ and control mice had a similar increase in the numbers of proliferating cell nuclear antigen–positive cells in response to Li^+. However, $AC6^{loxloxCre}$ mice had a higher number of H^+-ATPase B1 subunit–positive cells under standard conditions and after Li^+ administration. Collectively, AC6 has a minor role in Li-NDI development but may be important for determining the intercalated cell–to–principal cell ratio.

JCI insight

RESEARCH ARTICLE

Role of adenylyl cyclase 6 in the development of lithium-induced nephrogenic diabetes insipidus

Søren Brandt Poulsen,[1,2] Tina Bøgelund Kristensen,[1] Heddwen L. Brooks,[3] Donald E. Kohan,[4] Timo Rieg,[2,5] and Robert A. Fenton[1]

[1]InterPrET Center, Department of Biomedicine, Aarhus University, Aarhus, Denmark. [2]VA San Diego Healthcare System, San Diego, California, USA. [3]Department of Physiology, College of Medicine, University of Arizona, Tucson, Arizona, USA. [4]Division of Nephrology, University of Utah Health Sciences Center, Salt Lake City, Utah, USA. [5]Department of Medicine, University of California, San Diego, La Jolla, California, USA.

Psychiatric patients treated with lithium (Li^+) may develop nephrogenic diabetes insipidus (NDI). Although the etiology of Li^+-induced NDI (Li-NDI) is poorly understood, it occurs partially due to reduced aquaporin-2 (AQP2) expression in the kidney collecting ducts. A mechanism postulated for this is that Li^+ inhibits adenylyl cyclase (AC) activity, leading to decreased cAMP, reduced AQP2 abundance, and less membrane targeting. We hypothesized that Li-NDI would not develop in mice lacking AC6. Whole-body AC6 knockout ($AC6^{-/-}$) mice and potentially novel connecting tubule/principal cell–specific AC6 knockout ($AC6^{loxloxCre}$) mice had approximately 50% lower urine osmolality and doubled water intake under baseline conditions compared with controls. Dietary Li^+ administration increased water intake and reduced urine osmolality in control, $AC6^{-/-}$, and $AC6^{loxloxCre}$ mice. Consistent with $AC6^{-/-}$ mice, medullary AQP2 and pS256-AQP2 abundances were lower in $AC6^{loxloxCre}$ mice compared with controls under standard conditions, and levels were further reduced after Li^+ administration. $AC6^{loxloxCre}$ and control mice had a similar increase in the numbers of proliferating cell nuclear antigen–positive cells in response to Li^+. However, $AC6^{loxloxCre}$ mice had a higher number of H^+-ATPase B1 subunit–positive cells under standard conditions and after Li^+ administration. Collectively, AC6 has a minor role in Li-NDI development but may be important for determining the intercalated cell–to–principal cell ratio.

Introduction

Despite lithium (Li^+) usage being associated with renal, neurological, and endocrine side effects, the drug is still frequently used for the treatment of psychological disorders, e.g., bipolar disorder (1). The most common adverse effect of Li^+ therapy, affecting approximately 50% of patients, is Li^+-induced nephrogenic diabetes insipidus (Li-NDI), characterized by polydipsia, polyuria, and a limited renal response to the antidiuretic hormone, arginine vasopressin (AVP) (2). The polyuric effects of Li^+ are associated with a marked decrease in the abundance of the water channel aquaporin-2 (AQP2) in collecting duct (CD) principal cells (PCs), accompanied by a large increase in the ratio of intercalated cells (ICs) to PCs along the CD system (3, 4). Furthermore, long-term (chronic) Li^+ therapy increases the possibility of developing end-stage renal disease and is associated with an increased incidence of developing solid renal tumors (discussed in ref. 5). Despite these side effects, Li^+ therapy is continued for the majority of patients with Li-NDI, as the patient's quality of life is greatly affected by side effects, e.g., bipolar disorder symptoms. Thus, understanding the complete mechanism(s) of Li-NDI and developing ways to reverse the AVP resistance of the CD following Li^+ treatment are the first steps to newer and safer therapies for psychological disorders.

A multitude of studies have been performed to identify the altered cellular signaling events that underlie Li-NDI (discussed in ref. 6). However, despite major progress, no clear consensus regarding the "trigger" for the onset of the condition exists. For example, data from large-scale proteomic (7) and metabonomic approaches (8), coupled with targeted studies in animal models and gene-modified mice, have illustrated changes in renal prostaglandins (9); purinergic signaling (10); and the activity of glycogen synthase kinase 3 (GSK3) (11), PKC (12), MAPKs, ERKs ERK1/2 and P38α (13), and the phosphatidylinositol signal-

Authorship note: T. Rieg and R.A. Fenton contributed equally to this work as senior authors.

Conflict of interest: The authors have declared that no conflict of interest exists.

Submitted: October 4, 2016
Accepted: February 21, 2017
Published: April 6, 2017

Reference information:
JCI Insight. 2017;2(7):e91042. https://doi.org/10.1172/jci.insight.91042.

Table 1. Body weight and plasma [Li⁺] in AC6$^{-/-}$ mice versus WT mice and AC6$^{loxlox Cre}$ mice versus AC6^{loxlox} mice under baseline conditions and Li⁺ administration

Parameter	WT		AC6$^{-/-}$		AC6^{loxlox}		AC6$^{loxlox Cre}$	
	Baseline	Li⁺ (27 days)	Baseline	Li⁺ (27 days)	Baseline	Li⁺ (15 days)	Baseline	Li⁺ (15 days)
BW (g)	24.4 ± 0.8 (8)	25.9 ± 0.7 (8)[A]	24.2 ± 0.9 (8)	26.0 ± 0.7 (6)[B]	33.3 ± 1.5 (9)	30.7 ± 1.2 (9)[C]	28.5 ± 2.7 (5)	27.0 ± 1.9 (5)[D]
Plasma [Li⁺] (mM)	0.06 ± 0.02 (8)	0.72 ± 0.04[A] (8)	0.10 ± 0.02 (8)	0.94 ± 0.06[B,E] (6)	NM	0.75 ± 0.09 (5)	NM	0.64 ± 0.09 (5)

[A]WT baseline versus WT Li⁺, $P < 0.05$; [B]AC$^{-/-}$ baseline versus AC6$^{-/-}$ Li⁺, $P < 0.05$; [C]AC6^{loxlox} baseline versus AC6^{loxlox} Li⁺, $P < 0.05$; [D]AC6$^{loxlox Cre}$ baseline versus AC6$^{loxlox Cre}$ Li⁺, $P < 0.05$; [E]WT Li⁺ versus AC6$^{-/-}$ Li⁺, $P < 0.05$. Values are mean ± SEM. Numbers in parentheses represent number of observations per condition (n). NM, not measured.

ing pathway and the Wingless-Int/β-catenin (Wnt/β-catenin) pathway (7) among others, during Li-NDI. However, due to its role as the major downstream signaling molecule of AVP and its capacity to modulate several of the altered signaling pathways described above, diminished levels/effects of cAMP are thought to be the *primary* cause of Li-NDI. This essential role of cAMP in Li-NDI is supported by the following: (a) Li⁺ can directly inhibit adenylyl cyclases (ACs) (14, 15); (b) the AVP-induced water permeability of isolated perfused rabbit cortical CDs is reduced in the presence of Li⁺ but overcome in the presence of exogenous cAMP (16); (c) in response to AVP or direct activation of AC by forskolin, cAMP accumulation in CDs isolated from Li⁺-treated rats is severely reduced (17); and (d) inhibition of the Li⁺ target GSK3β reduces AVP-induced AC activity and cAMP generation in CD cells (18).

AC6 is the most abundantly expressed AC isoform in the mouse inner medulla (IM), and we have previously demonstrated that mice lacking AC6 (AC6$^{-/-}$) have dramatically reduced IM cAMP levels, which are not significantly increased following forskolin or AVP stimulation (19). Furthermore, AC6$^{-/-}$ mice have reduced AQP2 phosphorylation/trafficking and suffer from NDI, highlighting an essential role of AC6 for the AVP-cAMP axis and urinary concentration. Therefore, due to the proposed essential role of reduced cAMP levels in the onset of Li-NDI and evidence that Li⁺ preferentially inhibits AC6 (20), we hypothesized in this study that Li-NDI would not develop in total body AC6 knockout (AC6$^{-/-}$) mice. However, our results demonstrate that, in AC6$^{-/-}$ mice and connecting tubule/PC-specific AC6 knockout (AC6$^{loxlox Cre}$) mice, dietary Li⁺ administration has similar effects on renal water handling and AQP2 levels relative to control mice. Our studies demonstrate that in vivo AC6 and IM cAMP generation play a minor role in the development of Li-NDI but point toward AC6 playing a role for cellular proliferation.

Results

Li⁺ reduces urine osmolality and increases water intake in AC6$^{-/-}$ and WT mice. To test the contribution of AC6 to Li-NDI, AC6$^{-/-}$ mice and WT littermates were initially fed a standard diet (baseline) and then shifted to a Li⁺-containing diet for 27 days. AC6$^{-/-}$ and WT mice developed NDI, as evidenced by reduced urine osmolality and increased water intake (Figure 1, A and B, $P < 0.05$; for body weight and plasma [Li⁺], see Table 1). Baseline urine osmolality was lower in AC6$^{-/-}$ mice compared with WT mice (Figure 1A, $P < 0.05$), a difference that remained for the duration of the Li⁺ administration. After the initiation of Li⁺ administration, AC6$^{-/-}$ mice had significantly reduced urine osmolality on day 1, while a significant reduction in urine osmolality in WT mice was only observed from day 3 and onward (Figure 1A). Similarly, urine osmolality relative to baseline was significantly lower in AC6$^{-/-}$ mice on days 1 and 2 (Figure 1C, $P < 0.05$), after which no significant differences were observed. In agreement with the urine osmolality data, baseline water intake was significantly higher in AC6$^{-/-}$ mice, and this difference remained for the duration of the Li⁺ administration (Figure 1B, $P < 0.05$). Compared to baseline, Li⁺ induced a significantly higher water intake at an earlier time point in AC6$^{-/-}$ mice than in WT mice (day 4 and day 6, respectively, Figure 1B, $P < 0.05$). For the majority of the time points examined, no major differences between the genotypes in the fractional water intake relative to baseline were observed (Figure 1D).

AC6$^{loxlox Cre}$ mice have greater water intake and lower urine osmolality under baseline conditions. AC6 expression is heterogeneous in the kidney tubule (21), and we have previously demonstrated roles of AC6 in cells of the proximal tubule, thick ascending limb, and distal convoluted tubule (22, 23). Therefore, to isolate a potential role of AC6 in kidney and CD PCs, the main "target" cell for Li⁺ effects (24), we generated a condition-

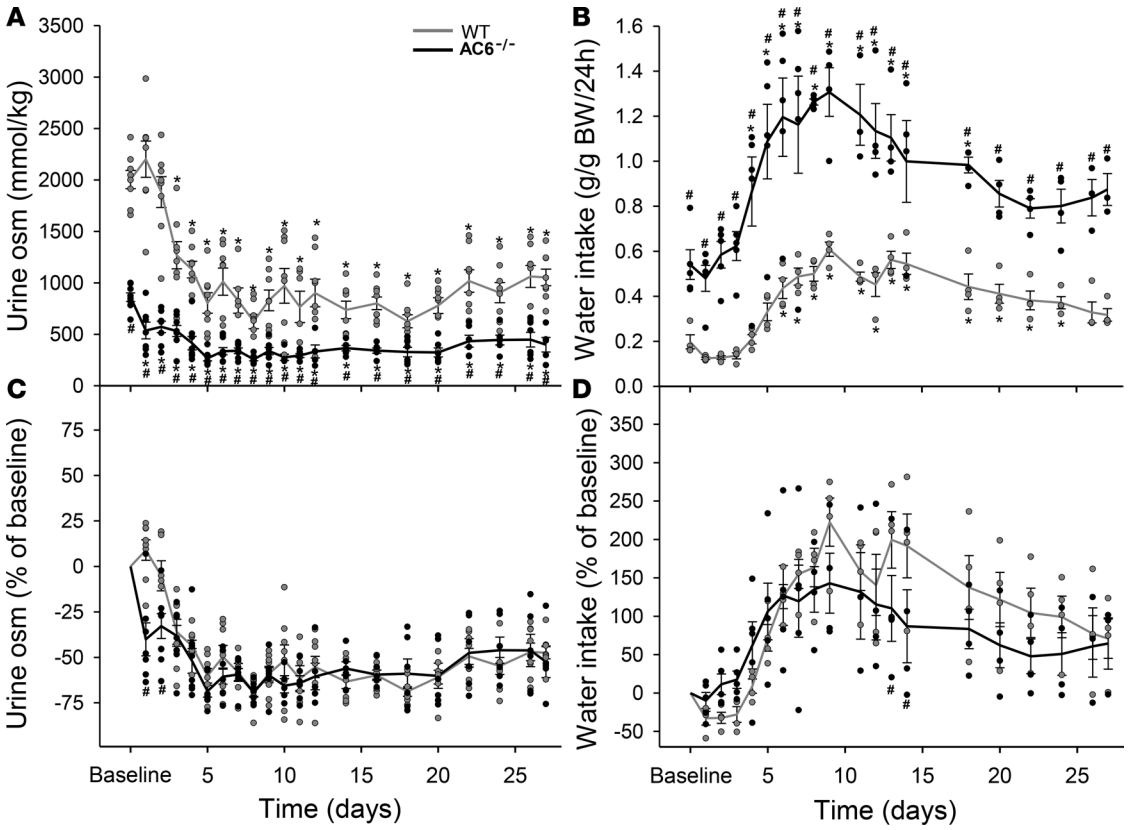

Figure 1. Li⁺ reduces urine osmolality and increases water intake in AC6$^{-/-}$ and WT mice. Following an initial baseline period on standard diet, mice lacking adenylyl cyclase 6 (AC6$^{-/-}$) and WT mice were fed a Li⁺-containing diet for 27 days, during which physiological parameters were measured. (**A**) Urine osmolality (osm), (**B**) water intake, (**C**) urine osmolality relative to baseline conditions (percentage of baseline), and (**D**) water intake relative to baseline conditions (percentage of baseline). Baseline values are averages of the last 5–7 days before switching from standard diet to Li⁺ diet. Sample size for urine osmolality: AC6$^{-/-}$, n = 5–8; WT, n = 6–8. Sample size for water intake: AC6$^{-/-}$, n = 3–5; WT, n = 4. Values are mean ± SEM. All statistical comparisons were performed using 2-way repeated-measurements ANOVA followed by Holm-Sidak post-hoc tests. *P < 0.05, baseline versus Li⁺ administration; #P < 0.05, AC6$^{-/-}$ versus WT at individual days.

al mouse model with AC6 deletion controlled by AQP2-dependent Cre recombinase expression (25). After several attempts with antibodies from various commercial sources, we identified an antibody that, in cortex homogenates from WT mice, detected AC6 as a smear centered at 150 kDa (26, 27). No signal was detectable in AC6$^{-/-}$ mice, demonstrating for the first time to our knowledge specificity of an AC6 antibody in Western blots (Figure 2A). In AC6^{loxloxCre} mice under baseline conditions, AC6 protein was approximately 50% reduced in IM homogenate compared with AC6^{loxlox} mice (Figure 2B, P < 0.05), a finding consistent and indicative of efficient AC6 knockout in PCs. No significant differences were detected in AC6 levels in the cortex and outer medulla/cortex (OM/cortex) homogenates (Figure 2B), presumably due to AC6 expression remaining in non-AQP2-expressing cells, which compose the vast majority of the cortex/outer stripe OM. Although labeling of AC6, using IHC, was unsuccessful (our unpublished observations), clear nuclear IHC labeling of Cre recombinase in both cortical, OM and IM collecting ducts in AC6^{loxloxCre} mice suggested successful deletion of AC6 in AQP2-expressing cells throughout the CD system (Figure 2, C–F). This is in agreement with previous IHC characterization of the *Aqp2-Cre* transgenic mouse line, demonstrating Cre expression specifically in connecting tubule (CNT) cells and CD PCs (28). Initial physiological characterization of body weight–matched mice (AC6^{loxloxCre}: 31.1 ± 2.3 g, ref. 9; AC6^{loxlox}: 33.3 ± 1.2 g, ref. 17) revealed lower urine osmolality and higher water intake in AC6^{loxloxCre} mice compared with AC6^{loxlox} mice (Figure 2G, P < 0.05). No significant differences were detected in food intake and plasma osmolality between the groups (Figure 2G).

Li⁺ reduces urine osmolality and increases water intake in AC6^{loxloxCre} and AC6^{loxlox} mice. To examine the contribution of AC6 to Li-NDI specifically in CNT cells and CD PCs, AC6^{loxloxCre} and AC6^{loxlox} mice were initially fed a standard diet (baseline) and then were either shifted to a Li⁺-containing diet (Figure 3) or maintained on standard diet (Supplemental Figure 1; supplemental material available online with this article; https://

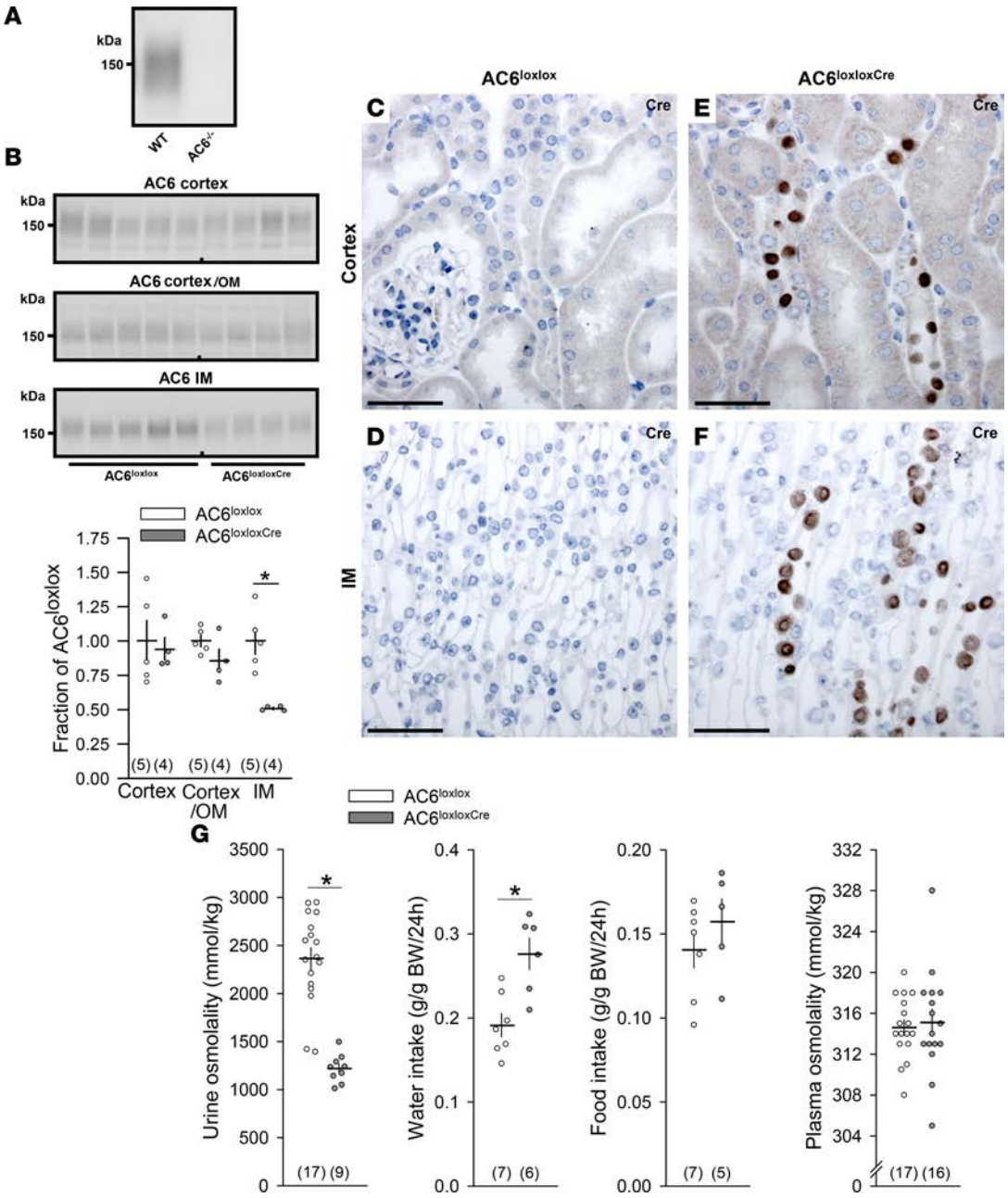

Figure 2. AC6^{loxloxCre} mice have greater water intake and lower urine osmolality under baseline conditions. A mouse model with deletion of adenylyl cyclase 6 (AC6) in aquaporin-2–expressing (AQP2-expressing) cells (AC6^{loxloxCre}) was generated as described in Methods. (**A**) AC6 was detected using immunoblotting as a broad smear in cortex homogenates from WT mice, whereas no signal was detectable in mice lacking AC6 (AC6$^{-/-}$ mice), confirming antibody specificity. (**B**) Under baseline conditions, AC6 protein signal was approximately 50% less intense in inner medulla (IM) homogenates from AC6^{loxloxCre} mice compared with AC6^{loxlox} control mice, whereas no significant reductions could be observed in cortex or outer medulla (OM)/cortex homogenates. The samples were used for immunoblotting on Figure 5. (**C**–**F**) Cre recombinase IHC showed clear nuclear labeling in cortical and IM collecting ducts of AC6^{loxloxCre} mice. Scale bar: 50 μm. (**G**) Under baseline conditions, AC6^{loxloxCre} mice had lower urine osmolality and higher water intake than AC6^{loxlox} mice, while no significant differences were found in food intake or plasma osmolality. Values are mean ± SEM. Numbers in parentheses indicate sample sizes. Statistical comparisons were performed using Student's 2-tailed *t* tests (**B** [cortex and OM/cortex homogenates] and **G** [water intake, food intake, and plasma osmolality]) and Satterthwaite's 2-tailed unequal variance *t* test (**B** [IM homogenate] and **G** [urine osmolality]). *$P < 0.05$. Data on urine osmolality and water intake are equivalent to baseline data presented in Figure 3 and Supplemental Figure 1. Plasma osmolality data originate from a different cohort of mice.

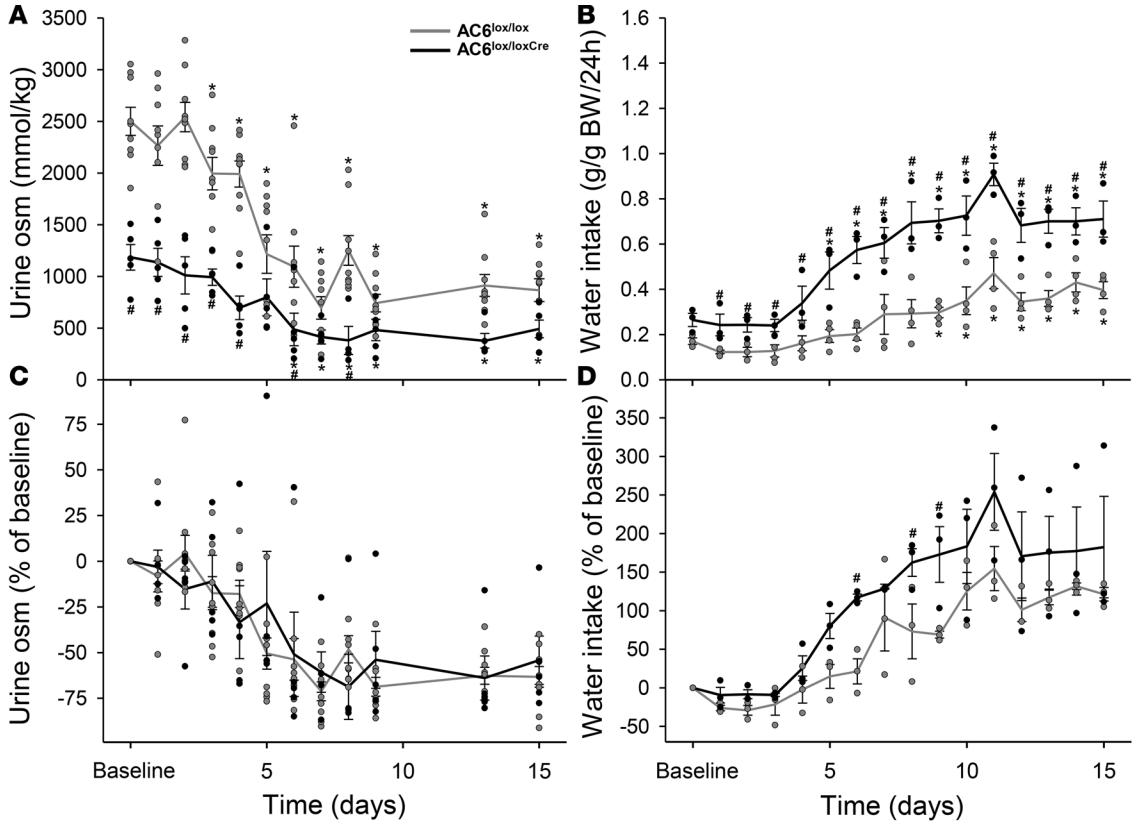

Figure 3. Li⁺ reduces urine osmolality and increases water intake in AC6^{loxloxCre} and AC6^{loxlox} mice. Following an initial baseline period on standard diet, mice with deletion of adenylyl cyclase (AC6) in aquaporin-2–expressing (AQP2-expressing) cells (AC6^{loxloxCre} mice) and AC6^{loxlox} control mice were fed a Li⁺-containing diet for 15 days. AC6^{loxloxCre} and AC6^{loxlox} mice were simultaneously maintained on the standard diet (Supplemental Figure 1). Physiological parameters were measured daily. (**A**) Urine osmolality (osm), (**B**) water intake, (**C**) urine osmolality relative to baseline conditions (percentage of baseline), and (**D**) water intake relative to baseline conditions (percentage of baseline). Baseline values are averages of the last 1–2 days before switching from standard to Li⁺ diet. Water intake and urine osmolality data on day 15 are equivalent to data presented in Figure 4. Sample size for urine osmolality: AC6^{loxloxCre}, n = 4–5; AC6^{loxlox}, n = 9. Sample size for water intake: AC6^{loxloxCre}, n = 3; AC6^{loxlox}, n = 4. Values are mean ± SEM. All statistical comparisons were performed using 2-way repeated-measurements ANOVA followed by Holm-Sidak post-hoc tests. *P < 0.05, baseline versus Li⁺ administration; #P < 0.05 AC6^{loxloxCre} versus AC6^{loxlox}.

doi.org/10.1172/jci.insight.91042DS1) for a total of 15 days. Both genotypes developed NDI in response to Li⁺, as evidenced by reduced urine osmolality and increased water intake (Figure 3, A and B). Baseline urine osmolality was lower in AC6^{loxloxCre} mice compared with AC6^{loxlox} mice (Figure 3A, P < 0.05), and this difference between the groups remained throughout the period of the Li⁺ administration (Figure 3A). In response to Li⁺, both AC6^{loxloxCre} and AC6^{loxlox} mice reduced their urine osmolality, but the time frame for these reductions to be significant was different between the groups (day 6 and day 3, respectively, Figure 3A, P < 0.05). No significant differences were detected between groups in the fractional urine osmolality relative to baseline (Figure 3C), suggesting an equivalent response to Li⁺ administration. Baseline water intake tended to be higher in AC6^{loxloxCre} mice (Figure 3B, P = 0.112), and it remained significantly higher for the duration of the Li⁺ administration (days 1–15, Figure 3B, P < 0.05). Water intake was increased in both AC6^{loxloxCre} and AC6^{loxlox} mice (day 5 and 9, respectively, Figure 3B, P < 0.05), with fractional water intake relative to baseline remaining higher in AC6^{loxloxCre} mice (Figure 3D, P < 0.05). Other physiological parameters on day 15 (study endpoint) are shown in Table 1 and Figure 4.

Li⁺ induces greater reductions in AQP2 and pS256-AQP2 abundances than genetic deletion of AC6. The molecular response to 15 days of Li⁺ administration in AC6^{loxloxCre} and AC6^{loxlox} mice was examined by immunoblotting kidney homogenates for various membrane proteins important for water and NaCl transport. In the IM, AC6 levels were significantly lower in AC6^{loxloxCre} mice (Figure 5, P < 0.05; see complete unedited blots in the supplemental material.). Li⁺ administration further reduced the IM AC6 levels in both genotypes, suggesting an effect of Li⁺ on AC6 abundance in AQP2-negative tissues/cells, such as ICs, thin descending or ascending limbs, blood vessels, or connective tissue. In agreement with our previous stud-

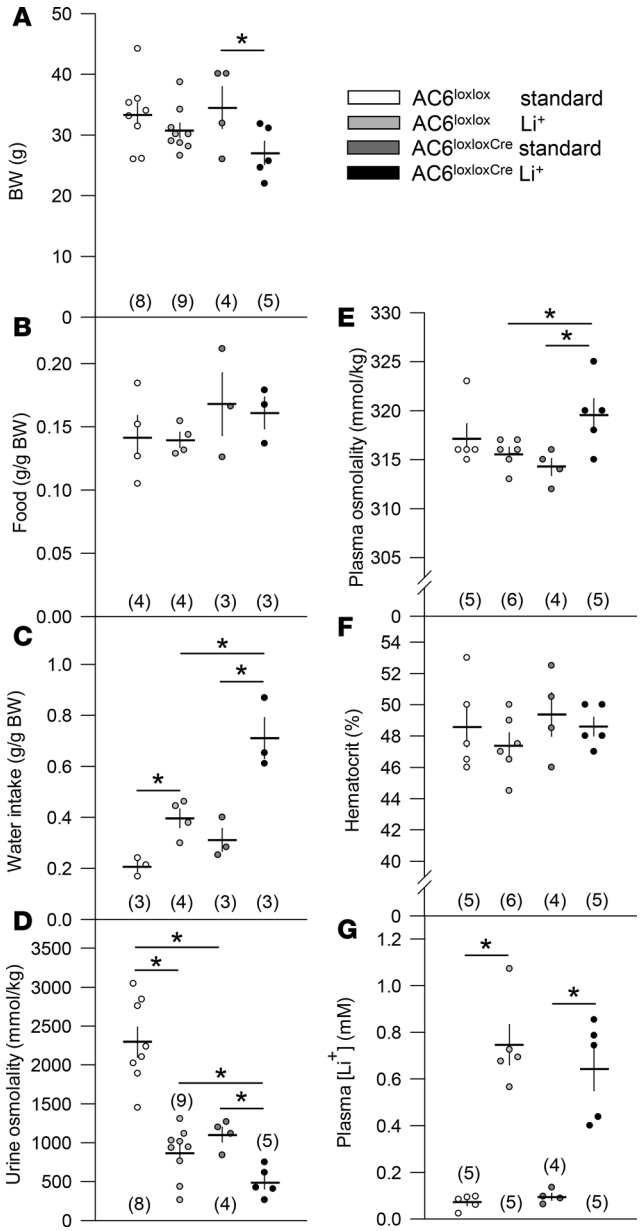

Figure 4. Li⁺ induces lower urine osmolality and higher water intake in AC6^{loxloxCre} and AC6^{loxlox} mice compared with standard diet. Following an initial baseline period on standard diet, mice with deletion of AC6 in AQP2-expressing cells (AC6^{loxloxCre} mice) and AC6^{loxlox} control mice were either fed a standard diet or a Li⁺-containing diet for 15 days (study endpoint). Presented are summary data for (**A**) body weight, (**B**) food intake, (**C**) water intake, (**D**) urine osmolality, (**E**) plasma osmolality, (**F**) hematocrit, and (**G**) plasma [Li⁺]. Data on water intake and urine osmolality are equivalent to data on day 15 presented in Figure 3 and Supplemental Figure 1. Values are mean ± SEM. Numbers in parentheses indicate sample sizes. All statistical comparisons were performed using 2-way ANOVA followed by Holm-Sidak post-hoc tests. *$P < 0.05$.

ies on AC6$^{-/-}$ mice (19), AC6^{loxloxCre} mice had significantly lower IM abundances of AQP2, pS256-AQP2, and pS269-AQP2 compared with AC6^{loxlox} mice (Figure 5, $P < 0.05$). Dietary Li⁺ intake further reduced AQP2 and pS256-AQP2 levels in AC6^{loxloxCre} and AC6^{loxlox} mice (Figure 5, $P < 0.05$), whereas pS269-AQP2 abundance following Li⁺ administration was reduced only in AC6^{loxlox} mice to levels similar to AC6^{loxloxCre} mice under baseline conditions. The levels of pS9-GSK3β, an inhibitory site on GSK3β that may be involved in development of Li-NDI, were significantly higher in Li⁺-administered AC6^{loxloxCre} and AC6^{loxlox} mice (Figure 5, $P < 0.05$). In cortex homogenates, significant reductions in AQP2 and pS256-AQP2 abundances were detected following Li⁺ administration (Figure 6, $P < 0.05$), alongside decreased levels of cleaved αENaC and γENaC (Figure 6, $P < 0.05$). Similar changes in AQP2 profiles were observed in the OM/cortex (Figure 7, $P < 0.05$). Neither Li⁺ diet nor genotype had any effect on the abundances of NCC, NKCC2, and pT96/T101-NKCC2 (Figures 6 and 7, $P < 0.05$). Combined, these data indicate that dietary Li⁺ intake has a greater effect on AQP2 and pS256-AQP2 abundances and the levels of cleaved αENaC and γENaC than genetic deletion of AC6 alone.

Li⁺ increases the number of PCNA-positive cells in IMCD$_1$ in AC6^{loxloxCre} and AC6^{loxlox} mice and enhances IC numbers in AC6^{loxloxCre} mice. Li⁺ administration is known to induce cell proliferation (3, 29, 30). We examined the contribution of AC6 to this phenomenon by determining the levels of proliferating cell nuclear antigen (PCNA) in kidneys from AC6^{loxloxCre} and AC6^{loxlox} mice fed a standard diet or a Li⁺-containing diet for 15 days. Li⁺ administration increased the numbers of PCNA-positive cells in both genotypes, as demonstrated by greater total PCNA protein abundance in IM homogenates (Figure 5, $P < 0.05$) and a higher proportion of cells in the IMCD$_1$ (at the base of IM) expressing PCNA (Figure 8, A–I). Furthermore, a higher proportion of the PCNA-positive cells was AQP2 positive versus H⁺-ATPase B1 subunit positive in both genotypes (Figure 8J, $P < 0.05$). However, this difference was less pronounced in AC6^{loxloxCre} mice, in which fewer of the PCNA-labeled cells were AQP2 positive and more PCNA-labeled cells were H⁺-ATPase B1 subunit positive compared with AC6^{loxlox} mice (Figure 8J, $P < 0.05$). The Li⁺-administered AC6^{loxloxCre} mice showed a lower proportion of AQP2-positive cells and a higher proportion of H⁺-ATPase B1 subunit–positive cells in IMCD$_1$ compared with mice fed a standard diet (Figure 8K, $P < 0.05$), whereas these changes were not observed in AC6^{loxlox} mice (Figure 8K). In terms of PCNA-positive cells, we corrected for the difference in the number of AQP2-positive and H⁺-ATPase B1 subunit–positive cells by calculating the proportion of AQP2-positive and H⁺-ATPase B1 subunit–positive cells that were expressing PCNA. AC6^{loxlox} mice showed a higher proportion of AQP2-positive cells expressing PCNA compared with H⁺-ATPase B1 subunit–positive cells (Figure 8L, $P < 0.05$), whereas no effect was found in AC6^{loxloxCre} mice (Figure 8L). In both genotypes, H⁺-ATPase B1 subunit–positive cells were frequently situated next to each other in rows in the IMCD$_1$ (Figure 8, F, H and M), a finding which was not observed in mice fed a standard diet (Figure 8, E, G and M). There were no clear differences in the number of cells coexpressing AQP2 and the H⁺-ATPase B1 subunit under standard conditions or after Li⁺ administration (data not shown) (31, 32).

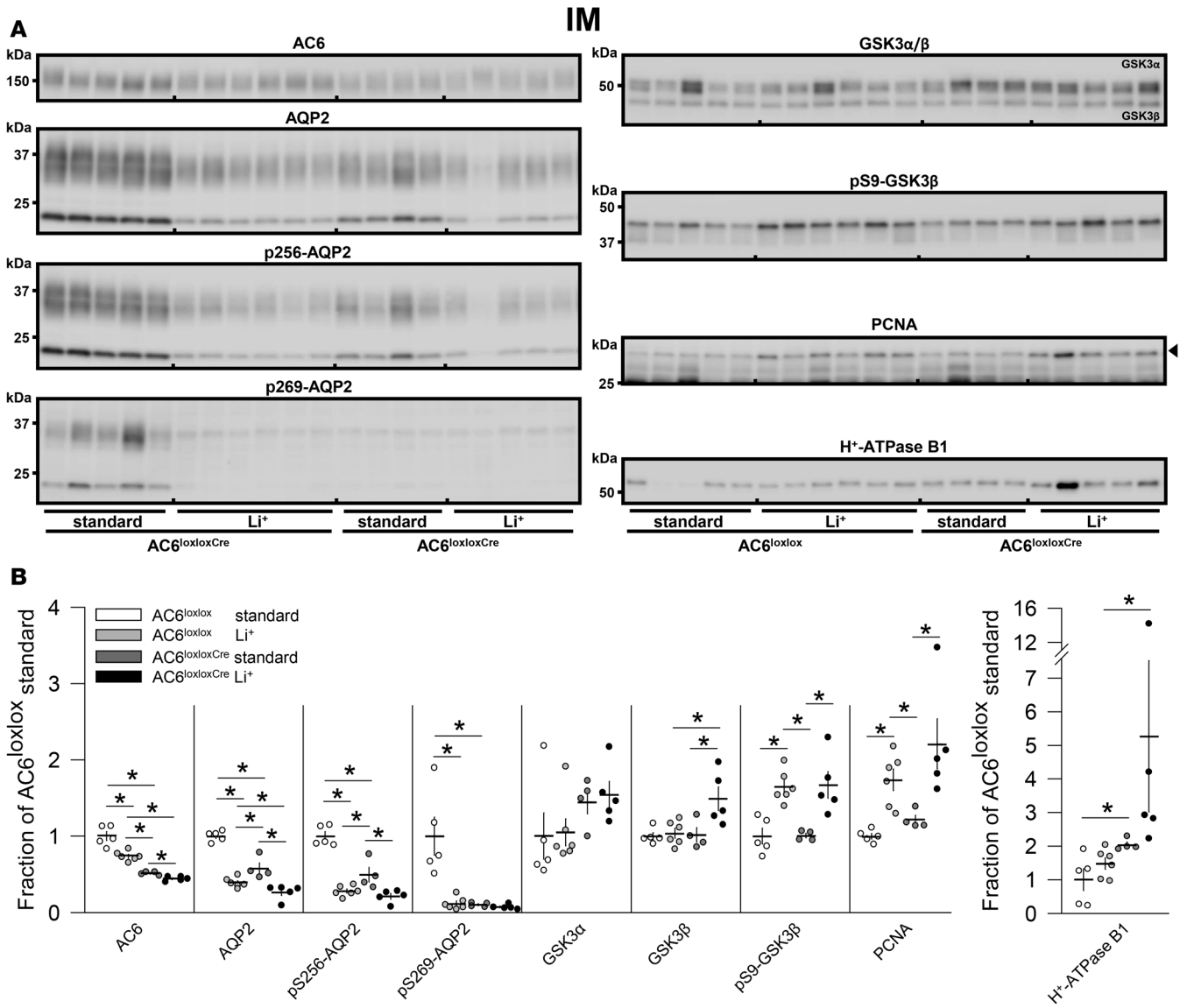

Figure 5. Li⁺ reduces inner medullary AQP2 and pS256-AQP2 abundances in AC6^{loxloxCre} and AC6^{loxlox} mice. (A) Semiquantitative immunoblotting of inner medulla (IM) homogenates from mice with deletion of adenylyl cyclase 6 (AC6) in aquaporin-2–expressing (AQP2-expressing) cells (AC6^{loxloxCre}) and AC6^{loxlox} control mice using antibodies targeting various proteins modulated during Li⁺-induced nephrogenic diabetes insipidus. (**B**) Summary data demonstrate that AC6, AQP2, pS256-AQP2, and pS269-AQP2 levels were significantly lower in AC6^{loxloxCre} mice relative to AC6^{loxlox} mice under standard conditions. Dietary Li⁺ administration further reduced AQP2 and pS256-AQP2 levels in AC6^{loxloxCre} and AC6^{loxlox} mice, indicating AC6-independent effects. pS9-glycogen synthase kinase 3 β (GSK3β) and proliferating cell nuclear antigen (PCNA) levels were significantly increased following Li⁺ administration in both genotypes. The samples from AC6^{loxloxCre} and AC6^{loxlox} mice on standard diet were used for immunoblotting in Figure 2. Values are mean ± SEM. Sample sizes: AC6^{loxlox} standard = 5, AC6^{loxlox} Li⁺ = 6, AC6^{loxloxCre} standard = 4, AC6^{loxloxCre} Li⁺ = 5. All statistical comparisons were performed using 2-way ANOVA followed by Holm-Sidak post-hoc tests. *$P < 0.05$.

Discussion

The most frequent side effect of Li⁺ therapy is NDI. Li⁺ interferes with the signal-transduction pathway of AVP, resulting in reduced AVP sensitivity in CD PCs and diminished levels of AQP2 expression (33). This reduced expression, coupled with reduced phosphorylation (34) at essential activation sites (35), is likely to be the major cell biological mechanism underlying Li-NDI. However, how Li⁺ therapy inhibits the signal-transduction pathway of AVP is not clear. One mechanism postulated for these effects is that Li⁺ inhibits the activity of ACs, leading to decreased cAMP production and ultimately decreased gene transcription and cAMP-dependent phosphorylation of AQP2. However, the major finding of the current study that Li⁺ treatment induces NDI of a similar magnitude in AC6$^{-/-}$ mice and control mice suggests that in vivo AC6 and medullary cAMP generation play a minor role in the development of Li-NDI.

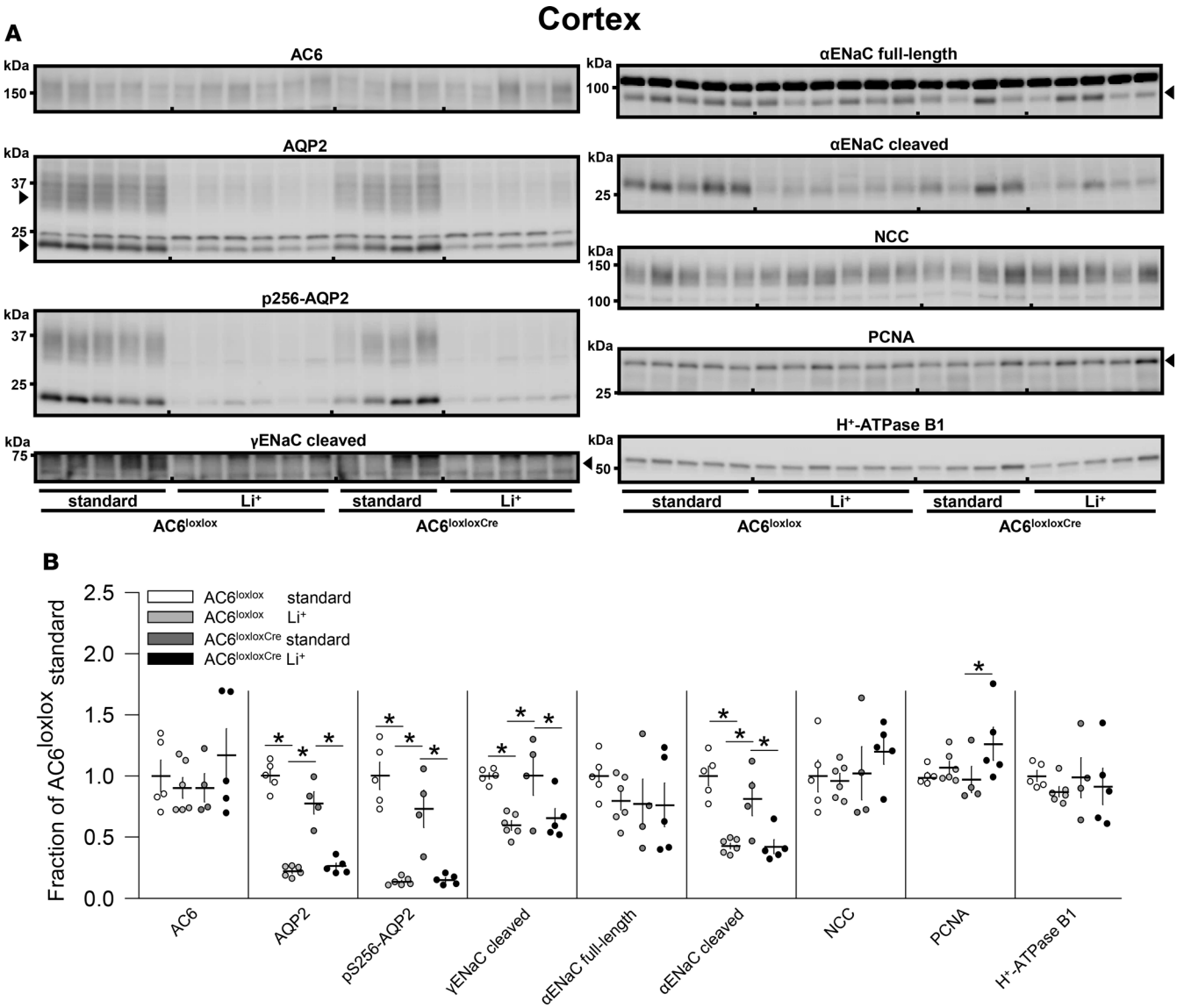

Figure 6. Li^+ reduces cortical AQP2, pS256-AQP2, cleaved αENaC, and cleaved γENaC abundances in $AC6^{loxloxCre}$ and $AC6^{loxlox}$ mice. (**A**) Semiquantitative immunoblotting of cortex homogenates from mice with deletion of adenylyl cyclase 6 (AC6) in aquaporin-2–expressing (AQP2-expressing) cells ($AC6^{loxloxCre}$ mice) and $AC6^{loxlox}$ controls using antibodies targeting various proteins modulated during Li^+-induced nephrogenic diabetes insipidus. (**B**) Summary data demonstrate lower abundances of AQP2, pS256-AQP2, cleaved α epithelial Na channel (αENaC), and cleaved γENaC in response to Li^+ administration in both genotypes. The abundances of these proteins were higher in $AC6^{loxloxCre}$ mice fed a standard diet than in $AC6^{loxlox}$ mice fed a Li^+ diet, indicating AC6-independent effects. Values are mean ± SEM. Sample sizes: $AC6^{loxlox}$ standard = 5, $AC6^{loxlox}$ Li^+ = 6, $AC6^{loxloxCre}$ standard = 4, $AC6^{loxloxCre}$ Li^+ = 5. All statistical comparisons were performed using 2-way ANOVA followed by Holm-Sidak post-hoc tests. *$P < 0.05$.

One of the major hurdles for determining a direct role of ACs and cAMP generation for the development of Li-NDI in vivo has been the lack of a suitable animal model. For example, several previous studies implicating a role for reduced cAMP in the onset of Li-NDI did not measure cAMP levels in vivo (12, 36), whereas a direct cause-effect correlation cannot be concluded from other models with diminished cAMP levels following Li^+ treatment (17) due to compensatory mechanisms, such as a negative-feedback response of cells to increased AVP levels (37). A strength of the current study was the use two different mouse models that lack AC6, the AC isoform mediating the majority of AVP-induced IM cAMP formation, allowing us to assess directly a role of cAMP in Li-NDI.

Similarly to $AC6^{-/-}$ mice (Figure 1), our conditional mouse model ($AC6^{loxloxCre}$ mice) with AC6 deletion specifically in CNT cells and CD PCs demonstrated key features of NDI, including significantly higher water intake and lower urine osmolality under baseline conditions. A minor limitation of our constitutive knockout model is that we cannot completely exclude that developmental and physiological compensatory mechanisms play a

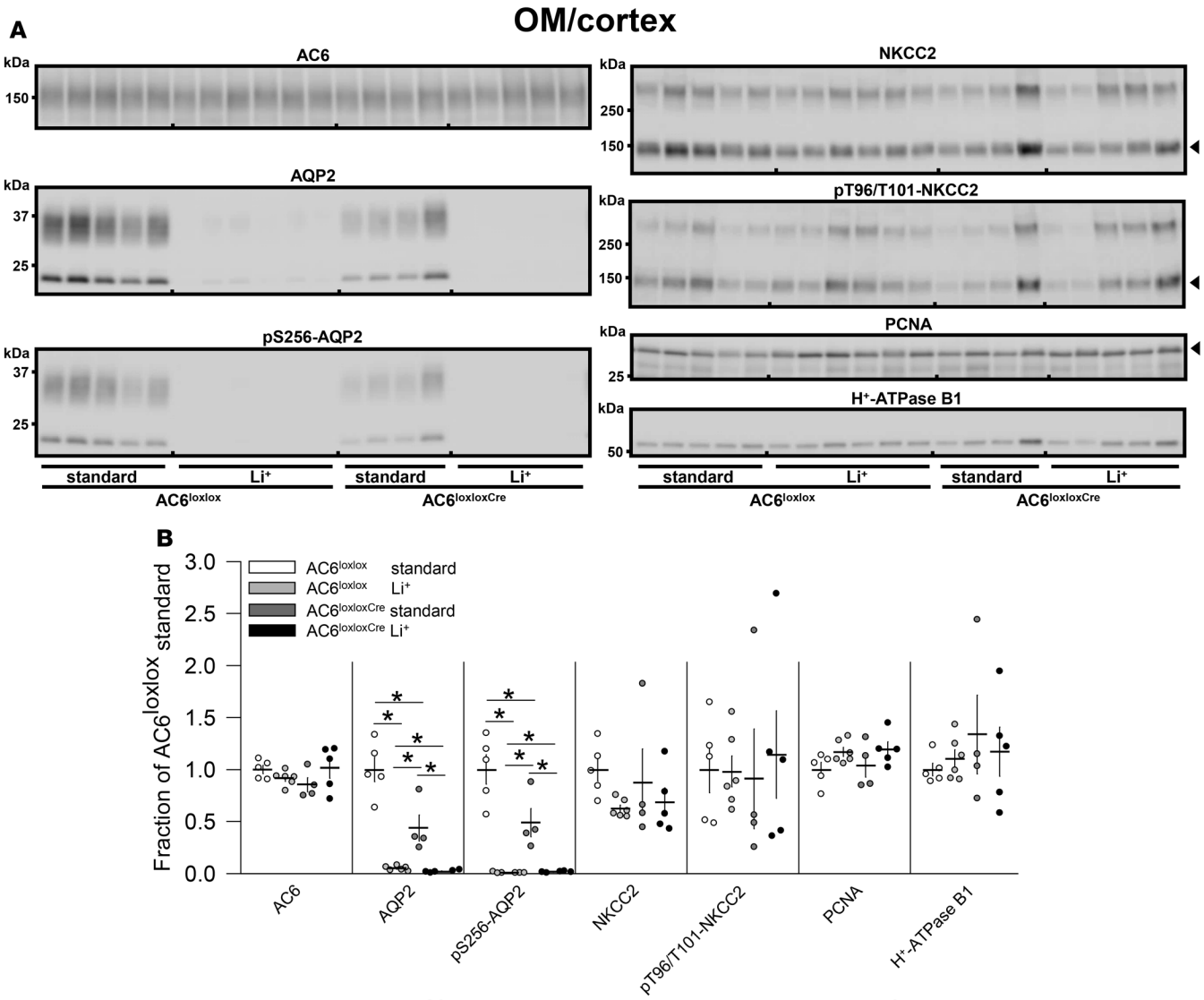

Figure 7. Li$^+$ reduces outer medullary/cortical AQP2 and pS256-AQP2 abundances in AC6^{loxloxCre} and AC6^{loxlox} mice. (**A**) Semiquantitative immunoblotting of outer medulla/cortex (OM/cortex) homogenates from mice with deletion of adenylyl cyclase 6 (AC6) in aquaporin-2–expressing (AQP2-expressing) cells (AC6^{loxloxCre} mice) and AC6^{loxlox} controls using antibodies targeting various proteins modulated during Li$^+$-induced nephrogenic diabetes insipidus. (**B**) Summary data demonstrate lower abundances of AQP2 and pS256-AQP2 in response to Li$^+$ administration in both genotypes. The abundances of these proteins were higher in AC6^{loxloxCre} mice fed a standard diet than in Li$^+$-administered AC6^{loxlox} mice, indicating AC6-independent effects. Values are mean ± SEM. Sample sizes: AC6^{loxlox} standard = 5, AC6^{loxlox} Li$^+$ = 6, AC6^{loxloxCre} standard = 4, AC6^{loxlox} Li$^+$ = 5. All statistical comparisons were performed using 2-way ANOVA followed by Holm-Sidak post-hoc tests. *$P < 0.05$.

role in some of the observed effects. However, with a phenotype closely resembling that of AC6$^{-/-}$ mice, the new model allowed us to examine the effect of Li-NDI following loss of AC6 specifically in the renal CD (19).

The current data using AC6^{loxloxCre} mice, coupled with our previous data (19), strengthen the theory that AC6 is responsible for AVP-mediated cAMP formation in the CD and, subsequently, the majority of cAMP-mediated effects in PCs. However, in AC6$^{-/-}$ and AC6^{loxloxCre} mice, dietary Li$^+$ intake for between 15 and 27 days resulted in further reductions in urine osmolality and increases in water intake. Although there was a delay of approximately 2 days in the renal response to dietary Li$^+$ intake in control mice (which we hypothesize is due to the time required for medullary osmolality gradients to be diminished), the overall reductions in urine osmolality and increases in water intake in both AC6 knockout models, relative to their respective baseline period, were of a similar magnitude to their respective control mice. Furthermore, Li$^+$ administration resulted in greater reductions in AQP2 and pS256-AQP2 abundances than observed with genetic deletion of AC6; hence, the isolated effect of Li$^+$ was greater than the effect of deleting AC6, sug-

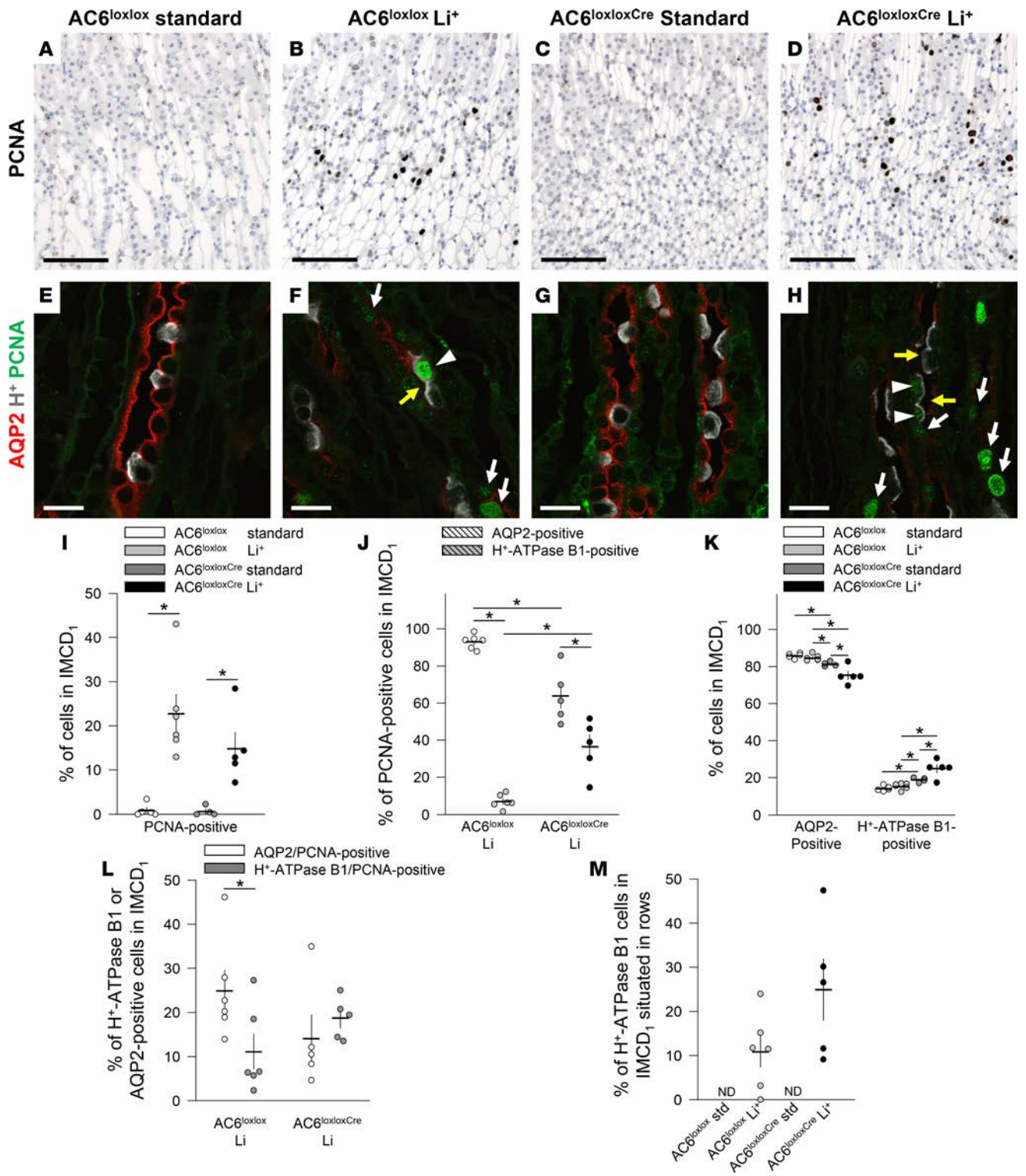

Figure 8. Li⁺ increases the number of PCNA-positive cells in $IMCD_1$ in $AC6^{loxloxCre}$ and $AC6^{loxlox}$ mice and enhances intercalated cell numbers in $AC6^{loxloxCre}$ mice. (**A**–**D**) Immunohistochemical labeling of proliferating cell nuclear antigen (PCNA) at the base of the inner medulla (IM) in mice with deletion of adenylyl cyclase 6 (AC6) in aquaporin-2–expressing (AQP2-expressing) cells ($AC6^{loxloxCre}$ mice) and $AC6^{loxlox}$ control mice following Li⁺ administration. Scale bar: 100 μm. (**E**–**H**) Immunohistochemical triple-fluorescence labeling in IM_1 for AQP2 (red), H⁺-ATPase B1 subunit (H⁺, gray), and PCNA (green). White arrows indicate PCNA/AQP2-positive cells, arrowheads indicate PCNA/H⁺-ATPase B1 subunit–positive cells, and yellow arrows indicate H⁺-ATPase–positive cells situated in rows. Scale bar: 20 μm. (**I**) Percentage of cells in $IMCD_1$ that were PCNA positive. (**J**) Percentage of PCNA-positive cells in $IMCD_1$ that were AQP2- positive or H⁺-ATPase B1 subunit positive. (**K**) Percentage of cells in $IMCD_1$ that were AQP2 positive or H⁺-ATPase B1 subunit positive. (**L**) Percentage of H⁺-ATPase B1 subunit– and AQP2-positive cells that showed PCNA labeling. (**M**) Percentage of H⁺-ATPase B1 subunit–positive cells situated in rows. Values are mean ± SEM. Mean number of cells counted per mouse ± SEM (*n*) were as follows: $AC6^{loxlox}$ standard: 254 ± 19 (5), $AC6^{loxlox}$ Li⁺: 372 ± 24 (6), $AC6^{loxloxCre}$ standard: 302 ± 30 (4); and $AC6^{loxloxCre}$ Li⁺: 441 ± 93 (5). Statistical comparisons were performed using 2-way ANOVA followed by Holm-Sidak post-hoc tests (**I** and **K**), 2-way repeated-measurements ANOVAs followed by Holm-Sidak post-hoc tests (**J** and **L**), or Student's 2-tailed *t* test (**M**). $^*P < 0.05$.

gesting that AC6- and cAMP-independent Li^+ effects on the signal-transduction pathway modulate AQP2 expression. Together, these data indicate that development of Li-NDI is independent of the actions of AC6 in CD PCs and, thus, cAMP. The current data are in line with a previous study performed in Brattleboro rats with clamped blood dDAVP levels, in which during Li-NDI there was no difference in dDAVP-generated cAMP generation or AQP2 levels in IMs compared with control Brattleboro rats (38).

Besides reduced AQP2 expression, in response to Li^+, the kidney CD "remodels," with an increased ratio of ICs to PCs (3). It is well established that Li^+ induces an increase in the numbers/percentages of both ICs and PCs expressing the proliferation marker, PCNA (3, 30). The increased PCNA expression is reduced by inhibiting the mTOR pathway, a controller of cell proliferation, whereas the inhibitory effect of Li^+ on GSK3β and AQP2 is unaffected by rapamycin (39). mTOR may also stimulate checkpoint kinase 1 (Chk1) and thereby prevent cell cycle progression through the G_2 phase (30, 40). Hence, this mechanism may underlie the higher number of PCs expressing PCNA during Li^+ administration. Li^+ also induces renal distal tubular acidosis (41, 42), a condition that in itself may result in IC proliferation (43). Thus, it could be speculated that, during Li^+ administration, PCNA-positive ICs are dividing in response to metabolic acidosis, while the majority of PCs expressing PCNA are arrested in the G_2 phase due to direct effects of Li^+ (30). Of note, after 14 days of NH_4Cl-induced acidosis, the percentage of ICs expressing PCNA in the OMCD was reported to be approximately 5-fold higher compared with the percentage of PCs (43). This is in contrast to the Li^+-induced (15 days) PCNA expression in our $AC6^{loxlox}$ control mice, in which the percentage of PCNA-positive PCs was significantly higher than the percentage of PCNA-positive ICs. Thus, Li^+-administered mice may show a higher number of PCs expressing PCNA compared with what would be expected during normal acidosis.

On standard diet, $AC6^{loxloxCre}$ mice had a higher IC-to-PC ratio compared with $AC6^{loxlox}$ mice, yet $AC6^{loxloxCre}$ mice did not present ICs in rows following Li^+ treatment, indicating the occurrence of two separate underlying mechanisms. It could be speculated that, while the Li^+-induced increase in IC-to-PC ratio was due to proliferation of ICs, the increased IC-to-PC ratio induced by AC6 deletion could be due to interconversion of PCs to ICs, as previously reported in K^+ depletion experiments (32). Thus, the combined effect of Li^+ and AC6 deletion could have a positively additive effect on the IC-to-PC ratio. Whether AC6 in the kidney is an indicator/modulator of differentiation as described in the mouse colon (44), in which AC6 is downregulated in the most differentiated surface cells, remains to be determined. However, based on the current data, it is plausible that AC6 plays distinctive roles in epithelial cell proliferation and may even be a determinant of the conversion of PC to IC (45). Examination of Li^+ effects in cell lineage–tracing models, or such models with an AC6-deficient background, would be a powerful approach to examine these possibilities (46, 47).

As highlighted in the Introduction, Li^+ acts as a counterregulator of AVP by modulating a variety of different pathways (7–13), but it is often thought that cAMP is the second messenger mediating these events. An example of this comes from recent studies indicating a role for the ubiquitously expressed GSK3, which is effectively inhibited by Li^+, in the onset of Li-NDI. GSK3β is suggested to be important for modulating AC activity, cAMP generation, and AVP sensitivity in the CD (18). However, GSK3α knockout mice, despite having impaired AVP-induced cAMP responses in CDs, are only mildly resistant to the onset of Li-NDI (48). Similarly, in the current study, although we saw clear inhibition of GSK3 activity (as evidenced by increased phosphorylation at an inhibitory site) following Li^+ administration, the developed Li-NDI must be cAMP independent. If Li-NDI can develop in the absence of AC6 and changes in cAMP, what is the mechanism? It is plausible that, due to its pleiotropic actions, inhibition of GSK3 will affect a number of cAMP-independent intracellular signaling cascades and is thus still a central player in development of Li-NDI. Furthermore, very recent studies have demonstrated that cAMP-independent pathways from the vasopressin type 2 receptor for AQP2 membrane targeting exist (49), which may also be disrupted by Li^+ treatment. Further studies are required to address the cAMP-independent signaling pathways involved in the development of Li-NDI.

In summary, our study shows that AC6 function and reduced cAMP levels are not major factors in the onset of Li-NDI. However, the data postulate a new function for AC6, in which it plays an instrumental role in determining the IC-to-PC ratios that occur during Li-NDI.

Methods

Generation and maintenance of AC6 knockout mouse models. $AC6^{-/-}$ mice were described previously (50), and WT littermates were used as controls. A conditional mouse model with AC6 constitutively deleted specifically in CNT cells and CD PCs (termed $AC6^{loxloxCre}$ mice) was generated by breeding transgenic mice in which exons 3–12 of the *Adcy6* gene were flanked by loxP sites (termed $AC6^{loxlox}$, ref. 51) with mice expressing Cre recom-

Table 2. Genotyping primers

Genotype	Forward	Reverse
WT	5′-AAGATCTGCTTTGTGGGTGC	5′-AGCCACTGGCTCGATTCGCGTGGCG
AC6$^{-/-}$	5′-GGAGACCTAGAGATGGAGTG	5′-GCCACTTGTGTAGCGCCAAG
AC6^{loxlox}	5′-GGAAAGTAGATCCTCGTCTCGG	5′-CCTACTTACAAGAACCGCAGGG
Aqp2-Cre	5′-AAGTGCCCACAGTCTAGCCTCT	5′-CCTGTTGTTCAGCTTGCACCAG 5′-GGAGAACGCTATGGACCGGAGT

binase (codon improved) under the regulatory elements of the *Aqp2* gene (25, 28). Mice were housed at approximately 20°C under a 12-hour-light/dark cycle in standard mouse cages with free access to tap water and standard rodent chow (0.8% NaCl, TD.7001, Harlan Teklad). Genotyping was performed by PCR analyses of ear biopsies (for primers, see Table 2).

Animal experimental protocols and urine and plasma analyses. All experiments were conducted in regular cages. Following an initial baseline period on standard rodent chow (0.8% NaCl, TD.7001, Harlan Teklad), AC6$^{-/-}$ and WT mice were shifted to a Li^+-containing diet (0.2% LiCl [40 mmol/kg], Harlan Teklad, TD09326) for 27 days. Body weight as well as water and food intake was determined, and urine was collected via reflex urination. Similarly, AC6^{loxloxCre} and AC6^{loxlox} mice were followed under an initial baseline period on standard rodent chow and then either maintained on the standard diet or shifted to the Li^+ diet for a period of 15 days. Mice were not provided with salt blocks during the Li^+ administration, because this may lead to extensive salt intake. Except for one female in the AC6^{loxloxCre} standard group and one female in the AC6^{loxloxCre} Li^+ group, all mice were males. On day 15, mice were anesthetized with isoflurane**,** blood was sampled from the retrobulbar plexus, and one of the kidneys was removed for generation of immunoblotting samples. For IHC, mice were subsequently perfused through the left ventricle with 4% paraformaldehyde and the kidney was removed and post-fixed in 4% paraformaldehyde at 37°C for 1 hour, followed by post fixation at 4°C for 24 hours. Urine and plasma osmolalities were measured by vapor pressure (Vapro, Wescor), while plasma [Li^+] was determined using a commercial assay (Infinity Lithium Reagent, Beckman Coulter).

Semiquantitative immunoblotting. The kidney was dissected on ice into IM, cortex, and the remaining tissue (enriched for OM/cortex) and homogenized in cold buffer containing 250 mmol/l sucrose, 10 mmol/l triethanolamine, protease inhibitors (Sigma-Aldrich and Roche Applied Science, respectively), and phosphatase inhibitors (Thermo Scientific). The homogenates were centrifuged at 1,000 *g* for 10 minutes, after which the supernatants were processed for immunoblotting as previously described (52). PVDF membranes were incubated with primary antibodies targeting AC5/6 (sc-590, Santa Cruz; dilution 1:800), AQP2 (H7661, dilution 1:1,500) (53), AQP2 (9398, dilution 1:1,000) (54), pS256-AQP2 (K0307, dilution 1:500) (55), pS269-AQP2 (dilution 1:500) (54), H^+-ATPase B1 subunit (H7659, dilution 1:2,000) (3), PCNA (P8825; Sigma-Aldrich; dilution 1:3,000), αENaC (dilution 1:1,000, provided by Johannes Loffing, Institute of Anatomy, Zürich, Switzerland) (56), γENaC (5361, dilution 1:200) (57), NCC (SPC-402D; StressMarq Biosciences Inc.; dilution 1:1,000), NKCC2 (1495, dilution 1:100) (58, 59), pT96/T101-NKCC2 (9934, dilution 1:50) (60), GSK-3α/β antibody (0011-A, Santa Cruz, dilution 1:200), and pS9-GSK3β (5B3, 9323; Cell Signaling Technology Inc.; dilution 1:500). Secondary antibodies were from DAKO, and sites of antibody/antigen interaction were visualized using the Enhanced Chemiluminescence System (GE Healthcare) and an ImageQuant LAS 4000 imager (GE Healthcare). Densitometric analyses were performed using Image Studio Lite (Qiagen).

IHC. Kidney tissue was processed for paraffin embedding and labeling as previously described (61). Two-μm sections were single immunolabeled for light microscopy (Cre recombinase [Covance; dilution 1:5,000] and PCNA [P8825; Sigma-Aldrich, dilution 1:20,000]) and triple immunolabeled for confocal laser scanning microscopy (PCNA [dilution 1:5,000], AQP2 [7661, dilution 1:1,000] [ref. 54], and biotinylated H^+-ATPase B1 subunit [7659, dilution 1:50][ref. 3]). Imaging was performed using a Leica DMRE light microscope equipped with a digital camera (Leica) and a Leica TCS SL laser scanning confocal microscope and Leica confocal software (Leica). Brightness was digitally enhanced on presented images. Cell counting was performed on fluorescence images acquired from the first 250 μm of IM_1, starting at the transition from the inner stripe OM.

Statistics. Pairwise comparisons of data meeting the statistical assumptions of normality and variance homogeneity were performed using Student's 2-tailed *t* test, while data only meeting assumptions of normality were analyzed using Satterthwaite's 2-tailed unequal variance *t* test. Comparisons of more than two groups were performed using either a 2-way repeated-measurements ANOVA or a 2-way ANOVA. Data not meeting the assumptions of normality and variance homogeneity were ln or square root transformed, and proportional data were either logit or arcsin transformed (62). Analyses were carried out using Stata 12.0 (StataCorp) or SigmaPlot 12.0 (Systat Software Inc.) for Windows. Values are presented as individual data points and mean ± SEM. *P* values of less than 0.05 were considered significant.

Study approval. All animal experimentation was conducted in accordance with the *Guide for the Care and Use of Laboratory Animals* (National Academies Press. 2011) and was approved by the local institutional animal care and use committee (VA San Diego Healthcare System).

Author contributions

SBP, HLB, TR, and RAF conceived and designed the work. SBP, TBK, TR, and RAF contributed to the acquisition, analysis, or interpretation of data for the work. DEK provided a novel reagent. All authors drafted the work or revised it critically for important intellectual content and approved the final version of the manuscript.

Acknowledgments

We would like to acknowledge the technical assistance of Inger-Merete Paulsen. RAF is supported by the Novo Nordisk Foundation, the Lundbeck Foundation, and the Danish Medical Research Council. TR is supported by the National Institute of Diabetes and Digestive and Kidney Diseases (1R01DK110621-01), the O'Brien Center for Acute Kidney Injury Research (P30DK079337), the Diabetes Endocrinology Research Center (P30DK063491), the American Heart Association (15BGIA22410018), and Satellite Healthcare (a not-for-profit renal care provider).

Address correspondence to: Robert A. Fenton, Aarhus University, Institute for Biomedicine, Wilhelm Meyers Allé 3, Building 1233, DK-8000 Aarhus C, Denmark. Phone: 0045.87167671; E-mail: robert.a.fenton@biomed.au.dk. Or to: Timo Rieg, Department of Molecular Pharmacology and Physiology, Morsani College of Medicine, University of South Florida, 12901 Bruce B. Downs Boulevard, MDC 8, Tampa, Florida 33612, USA. Phone: 813.974.4538; E-mail: trieg@health.usf.edu.

TR's present address is: Department of Molecular Pharmacology and Physiology, Morsani College of Medicine, University of South Florida, Tampa, Florida, USA.

1. Rej S, Herrmann N, Shulman K. The effects of lithium on renal function in older adults--a systematic review. *J Geriatr Psychiatry Neurol*. 2012;25(1):51–61.
2. Moeller HB, Rittig S, Fenton RA. Nephrogenic diabetes insipidus: essential insights into the molecular background and potential therapies for treatment. *Endocr Rev*. 2013;34(2):278–301.
3. Christensen BM, Kim YH, Kwon TH, Nielsen S. Lithium treatment induces a marked proliferation of primarily principal cells in rat kidney inner medullary collecting duct. *Am J Physiol Renal Physiol*. 2006;291(1):F39–F48.
4. Christensen BM, Marples D, Kim YH, Wang W, Frøkiaer J, Nielsen S. Changes in cellular composition of kidney collecting duct cells in rats with lithium-induced NDI. *Am J Physiol, Cell Physiol*. 2004;286(4):C952–C964.
5. Alsady M, Baumgarten R, Deen PM, de Groot T. Lithium in the Kidney: Friend and Foe? *J Am Soc Nephrol*. 2016;27(6):1587–1595.
6. Kishore BK, Ecelbarger CM. Lithium: a versatile tool for understanding renal physiology. *Am J Physiol Renal Physiol*. 2013;304(9):F1139–F1149.
7. Nielsen J, Hoffert JD, Knepper MA, Agre P, Nielsen S, Fenton RA. Proteomic analysis of lithium-induced nephrogenic diabetes insipidus: mechanisms for aquaporin 2 down-regulation and cellular proliferation. *Proc Natl Acad Sci USA*. 2008;105(9):3634–3639.
8. Hwang GS, Yang JY, Ryu DH, Kwon TH. Metabolic profiling of kidney and urine in rats with lithium-induced nephrogenic diabetes insipidus by (1)H-NMR-based metabonomics. *Am J Physiol Renal Physiol*. 2010;298(2):F461–F470.
9. Jia Z, Wang H, Yang T. Mice lacking mPGES-1 are resistant to lithium-induced polyuria. *Am J Physiol Renal Physiol*. 2009;297(6):F1689–F1696.
10. Zhang Y, Nelson RD, Carlson NG, Kamerath CD, Kohan DE, Kishore BK. Potential role of purinergic signaling in lithium-induced nephrogenic diabetes insipidus. *Am J Physiol Renal Physiol*. 2009;296(5):F1194–F1201.
11. Rao R, et al. Lithium treatment inhibits renal GSK-3 activity and promotes cyclooxygenase 2-dependent polyuria. *Am J Physiol Renal Physiol*. 2005;288(4):F642–F649.
12. Sim JH, et al. Absence of PKC-alpha attenuates lithium-induced nephrogenic diabetes insipidus. *PLoS ONE*. 2014;9(7):e101753.
13. Trepiccione F, et al. Early targets of lithium in rat kidney inner medullary collecting duct include p38 and ERK1/2. *Kidney Int*. 2014;86(4):757–767.
14. Jackson BA, Edwards RM, Dousa TP. Lithium-induced polyuria: effect of lithium on adenylate cyclase and adenosine 3',5'-monophosphate phosphodiesterase in medullary ascending limb of Henle's loop and in medullary collecting tubules. *Endocrinology*. 1980;107(6):1693–1698.
15. Goldberg H, Clayman P, Skorecki K. Mechanism of Li inhibition of vasopressin-sensitive adenylate cyclase in cultured renal epithelial cells. *Am J Physiol*. 1988;255(5 Pt 2):F995–1002.
16. Cogan E, Abramow M. Inhibition by lithium of the hydroosmotic action of vasopressin in the isolated perfused cortical collecting tubule of the rabbit. *J Clin Invest*. 1986;77(5):1507–1514.
17. Christensen S, Kusano E, Yusufi AN, Murayama N, Dousa TP. Pathogenesis of nephrogenic diabetes insipidus due to chronic administration of lithium in rats. *J Clin Invest*. 1985;75(6):1869–1879.
18. Rao R, Patel S, Hao C, Woodgett J, Harris R. GSK3beta mediates renal response to vasopressin by modulating adenylate

cyclase activity. *J Am Soc Nephrol*. 2010;21(3):428–437.
19. Rieg T, et al. Adenylate cyclase 6 determines cAMP formation and aquaporin-2 phosphorylation and trafficking in inner medulla. *J Am Soc Nephrol*. 2010;21(12):2059–2068.
20. Mann L, Heldman E, Shaltiel G, Belmaker RH, Agam G. Lithium preferentially inhibits adenylyl cyclase V and VII isoforms. *Int J Neuropsychopharmacol*. 2008;11(4):533–539.
21. Chien CL, et al. Impaired water reabsorption in mice deficient in the type VI adenylyl cyclase (AC6). *FEBS Lett*. 2010;584(13):2883–2890.
22. Fenton RA, Murray F, Dominguez Rieg JA, Tang T, Levi M, Rieg T. Renal phosphate wasting in the absence of adenylyl cyclase 6. *J Am Soc Nephrol*. 2014;25(12):2822–2834.
23. Rieg T, Tang T, Uchida S, Hammond HK, Fenton RA, Vallon V. Adenylyl cyclase 6 enhances NKCC2 expression and mediates vasopressin-induced phosphorylation of NKCC2 and NCC. *Am J Pathol*. 2013;182(1):96–106.
24. Kortenoeven ML, Pedersen NB, Miller RL, Rojek A, Fenton RA. Genetic ablation of aquaporin-2 in the mouse connecting tubules results in defective renal water handling. *J Physiol (Lond)*. 2013;591(8):2205–2219.
25. Ronzaud C, et al. Impairment of sodium balance in mice deficient in renal principal cell mineralocorticoid receptor. *J Am Soc Nephrol*. 2007;18(6):1679–1687.
26. Wu GC, Lai HL, Lin YW, Chu YT, Chern Y. N-glycosylation and residues Asn805 and Asn890 are involved in the functional properties of type VI adenylyl cyclase. *J Biol Chem*. 2001;276(38):35450–35457.
27. Sabbatini ME, Gorelick F, Glaser S. Adenylyl cyclases in the digestive system. *Cell Signal*. 2014;26(6):1173–1181.
28. Christensen BM, et al. Sodium and potassium balance depends on αENaC expression in connecting tubule. *J Am Soc Nephrol*. 2010;21(11):1942–1951.
29. Rojek A, et al. Altered expression of selected genes in kidney of rats with lithium-induced NDI. *Am J Physiol Renal Physiol*. 2005;288(6):F1276–F1289.
30. de Groot T, et al. Lithium causes G2 arrest of renal principal cells. *J Am Soc Nephrol*. 2014;25(3):501–510.
31. Trepiccione F, Capasso G, Nielsen S, Christensen BM. Evaluation of cellular plasticity in the collecting duct during recovery from lithium-induced nephrogenic diabetes insipidus. *Am J Physiol Renal Physiol*. 2013;305(6):F919–F929.
32. Park EY, et al. Proposed mechanism in the change of cellular composition in the outer medullary collecting duct during potassium homeostasis. *Histol Histopathol*. 2012;27(12):1559–1577.
33. Marples D, Christensen S, Christensen EI, Ottosen PD, Nielsen S. Lithium-induced downregulation of aquaporin-2 water channel expression in rat kidney medulla. *J Clin Invest*. 1995;95(4):1838–1845.
34. Trepiccione F, et al. Early targets of lithium in rat kidney inner medullary collecting duct include p38 and ERK1/2. *Kidney Int*. 2014;86(4):757–767.
35. Moeller HB, Olesen ET, Fenton RA. Regulation of the water channel aquaporin-2 by posttranslational modification. *Am J Physiol Renal Physiol*. 2011;300(5):F1062–F1073.
36. Zhang Y, et al. P2Y12 receptor localizes in the renal collecting duct and its blockade augments arginine vasopressin action and alleviates nephrogenic diabetes insipidus. *J Am Soc Nephrol*. 2015;26(12):2978–2987.
37. Anai H, et al. Upregulation of the expression of vasopressin gene in the paraventricular and supraoptic nuclei of the lithium-induced diabetes insipidus rat. *Brain Res*. 1997;772(1-2):161–166.
38. Li Y, Shaw S, Kamsteeg EJ, Vandewalle A, Deen PM. Development of lithium-induced nephrogenic diabetes insipidus is dissociated from adenylyl cyclase activity. *J Am Soc Nephrol*. 2006;17(4):1063–1072.
39. Gao Y, Romero-Aleshire MJ, Cai Q, Price TJ, Brooks HL. Rapamycin inhibition of mTORC1 reverses lithium-induced proliferation of renal collecting duct cells. *Am J Physiol Renal Physiol*. 2013;305(8):F1201–F1208.
40. Selvarajah J, Elia A, Carroll VA, Moumen A. DNA damage-induced S and G2/M cell cycle arrest requires mTORC2-dependent regulation of Chk1. *Oncotarget*. 2015;6(1):427–440.
41. Perez GO, Oster JR, Vaamonde CA. Incomplete syndrome of renal tubular acidosis induced by lithium carbonate. *J Lab Clin Med*. 1975;86(3):386–394.
42. Roscoe JM, Goldstein MB, Halperin ML, Wilson DR, Stinebaugh BJ. Lithium-induced impairment of urine acidification. *Kidney Int*. 1976;9(4):344–350.
43. Duong Van Huyen JP, et al. GDF15 triggers homeostatic proliferation of acid-secreting collecting duct cells. *J Am Soc Nephrol*. 2008;19(10):1965–1974.
44. Choi LJ, et al. Coordinate down-regulation of adenylyl cyclase isoforms and the stimulatory G protein (G(s)) in intestinal epithelial cell differentiation. *J Biol Chem*. 2010;285(17):12504–12511.
45. Wu H, et al. Aqp2-expressing cells give rise to renal intercalated cells. *J Am Soc Nephrol*. 2013;24(2):243–252.
46. Rinkevich Y, et al. In vivo clonal analysis reveals lineage-restricted progenitor characteristics in mammalian kidney development, maintenance, and regeneration. *Cell Rep*. 2014;7(4):1270–1283.
47. Romagnani P, Rinkevich Y, Dekel B. The use of lineage tracing to study kidney injury and regeneration. *Nat Rev Nephrol*. 2015;11(7):420–431.
48. Nørregaard R, et al. Glycogen synthase kinase 3α regulates urine concentrating mechanism in mice. *Am J Physiol Renal Physiol*. 2015;308(6):F650–F660.
49. Olesen ET, Moeller HB, Assentoft M, MacAulay N, Fenton RA. The vasopressin type 2 receptor and prostaglandin receptors EP2 and EP4 can increase aquaporin-2 plasma membrane targeting through a cAMP-independent pathway. *Am J Physiol Renal Physiol*. 2016;311(5):F935–F944.
50. Tang T, et al. Adenylyl cyclase type 6 deletion decreases left ventricular function via impaired calcium handling. *Circulation*. 2008;117(1):61–69.
51. Roos KP, Strait KA, Raphael KL, Blount MA, Kohan DE. Collecting duct-specific knockout of adenylyl cyclase type VI causes a urinary concentration defect in mice. *Am J Physiol Renal Physiol*. 2012;302(1):F78–F84.
52. Poulsen SB, et al. Reducing αENaC expression in the kidney connecting tubule induces pseudohypoaldosteronism type 1 symptoms during K+ loading. *Am J Physiol Renal Physiol*. 2016;310(4):F300–F310.
53. Nielsen J, Kwon TH, Praetorius J, Frøkiaer J, Knepper MA, Nielsen S. Aldosterone increases urine production and decreases

apical AQP2 expression in rats with diabetes insipidus. *Am J Physiol Renal Physiol*. 2006;290(2):F438–F449.
54. Moeller HB, Aroankins TS, Slengerik-Hansen J, Pisitkun T, Fenton RA. Phosphorylation and ubiquitylation are opposing processes that regulate endocytosis of the water channel aquaporin-2. *J Cell Sci*. 2014;127(Pt 14):3174–3183.
55. Hoffert JD, et al. Vasopressin-stimulated increase in phosphorylation at Ser269 potentiates plasma membrane retention of aquaporin-2. *J Biol Chem*. 2008;283(36):24617–24627.
56. Sorensen MV, et al. Rapid dephosphorylation of the renal sodium chloride cotransporter in response to oral potassium intake in mice. *Kidney Int*. 2013;83(5):811–824.
57. Masilamani S, Kim GH, Mitchell C, Wade JB, Knepper MA. Aldosterone-mediated regulation of ENaC alpha, beta, and gamma subunit proteins in rat kidney. *J Clin Invest*. 1999;104(7):R19–R23.
58. Jensen AM, Nørregaard R, Topcu SO, Frøkiaer J, Pedersen M. Oxygen tension correlates with regional blood flow in obstructed rat kidney. *J Exp Biol*. 2009;212(19):3156–3163.
59. Ecelbarger CA, Terris J, Hoyer JR, Nielsen S, Wade JB, Knepper MA. Localization and regulation of the rat renal Na(+)-K(+)-2Cl- cotransporter, BSC-1. *Am J Physiol*. 1996;271(3 Pt 2):F619–F628.
60. Dimke H, et al. Acute growth hormone administration induces antidiuretic and antinatriuretic effects and increases phosphorylation of NKCC2. *Am J Physiol Renal Physiol*. 2007;292(2):F723–F735.
61. Moeller HB, Knepper MA, Fenton RA. Serine 269 phosphorylated aquaporin-2 is targeted to the apical membrane of collecting duct principal cells. *Kidney Int*. 2009;75(3):295–303.
62. Sokal RR, Rohlf FJ. *Biometry: the principles and practice of statistics in biological research*. New York, New York: W.H. Freeman and Company; 1995.